

Structure of Fully Hydrated Fluid Phase Lipid Bilayers with Monounsaturated Chains

Norbert Kučerka*, Stephanie Tristram-Nagle*, John F. Nagle*[†]

*Physics Department and [†]Biological Sciences Department, Carnegie Mellon University, Pittsburgh Pennsylvania, 15213, USA

Received: 22 September 2005/Revised: 18 October 2005

Abstract. Quantitative structures are obtained at 30°C for the fully hydrated fluid phases of palmitoylphosphatidylcholine (POPC), with a double bond on the *sn*-2 hydrocarbon chain, and for dierucoylphosphatidylcholine (di22:1PC), with a double bond on each hydrocarbon chain. The form factors $F(q_z)$ for both lipids are obtained using a combination of three methods. (1) Volumetric measurements provide $F(0)$. (2) X-ray scattering from extruded unilamellar vesicles provides $|F(q_z)|$ for low q_z . (3) Diffuse X-ray scattering from oriented stacks of bilayers provides $|F(q_z)|$ for high q_z . Also, data using method (2) are added to our recent data for dioleoylphosphatidylcholine (DOPC) using methods (1) and (3); the new DOPC data agree very well with the recent data and with (4) our older data obtained using a liquid crystallographic X-ray method. We used hybrid electron density models to obtain structural results from these form factors. The result for area per lipid (A) for DOPC $72.4 \pm 0.5 \text{ \AA}^2$ agrees well with our earlier publications, and we find $A = 69.3 \pm 0.5 \text{ \AA}^2$ for di22:1PC and $A = 68.3 \pm 1.5 \text{ \AA}^2$ for POPC. We obtain the values for five different average thicknesses: hydrophobic, steric, head-head, phosphate-phosphate and Luzzati. Comparison of the results for these three lipids and for our recent dimyristoylphosphatidylcholine (DMPC) determination provides quantitative measures of the effect of unsaturation on bilayer structure. Our results suggest that lipids with one monounsaturated chain have quantitative bilayer structures closer to lipids with two monounsaturated chains than to lipids with two completely saturated chains.

Key words: X-ray scattering — Phospholipid bilayer — Dierucoylphosphatidylcholine — Palmitoylphosphatidylcholine — Dioleoylphosphatidylcholine

— Unsaturated lipids — Bilayer structure — Area per lipid — Fully hydrated fluid phase

Introduction

The chemical composition of the fatty acid chains in lipids affects many properties of the lipid bilayers, which are the structural hosts for functional proteins in biomembranes. Precise information about the lipid bilayer structure is therefore necessary to better understand lipid-protein interactions with applications to lipid-based drug design and biomimetic material development. The most dramatic effect in the bilayer properties is that phospholipids with saturated chains undergo phase transitions into chain-ordered phases that are not viable for most biomembranes. Although transition temperatures are reduced by having shorter chain lengths in saturated lipids, the introduction of double bonds reduces the transition temperatures much more effectively and permits nature to use lipids with longer chains (Gennis, 1989).

Biomembranes comprise complex mixtures of lipids with varying degrees of unsaturation, including polyunsaturation of up to six double bonds per chain (Eldho et al., 2003). In this investigation, we report structural results for three fluid phase lipid bilayers containing unsaturated chains. Palmitoylphosphatidylcholine (POPC), the most abundant lipid in animal cell membranes (Tattrie, Bennett & Cyr, 1968), is a mixed-chain lipid, containing a saturated chain at the *sn*-1 position and an unsaturated chain at the *sn*-2 position, a configuration that is the most common in naturally occurring lipids (Hanahan, 1997). The two other lipids, dioleoylglycerophosphatidylcholine (DOPC) and dierucoylphosphatidylcholine (di22:1PC), both contain two identical chains, each with one *cis* unsaturated bond located eight carbons from the terminal methyl end. The erucoyl chain has four more carbons than the oleoyl chain in DOPC, thereby providing a

thicker bilayer. We will compare our results for these unsaturated lipids with our earlier studies on fluid phase saturated lipids.

This study focuses on the effect of double bonds on the quantitative structure of lipid bilayers. There are different measures of the thicknesses that are valuable for different purposes, the hydrophobic thickness for consideration of hydrophobic matching of proteins in membranes, the steric thickness for interaction with other bilayers or with macromolecules, the head-head or phosphate-phosphate thickness that emerges most strongly from structural studies and the Luzzati thickness for the simplest volume-based picture of membranes. These are all related, through volumetric considerations to the unique area (A) per lipid parallel to the membrane surface. A is valuable for setting up or evaluating molecular dynamics simulations.

Recent advances in X-ray structure methodology allow us to obtain better results for these quantities (Zhang et al., 1996; Petrache, Feller & Nagle, 1997). Samples of fully hydrated, fluctuating arrays of fluid phase bilayers inherently have stacking and undulation disorder that prevents the acquisition of suitable data for successful application of traditional crystallographic analysis (Torbet & Wilkins, 1976). This same disorder, however, produces copious diffuse scattering that we have shown provides considerably more information than can be obtained from the traditional focus on Bragg peaks (Lyatskaya et al., 2001; Liu & Nagle, 2004). We have also added complementary X-ray data from unilamellar vesicles (ULVs), which do not have the disorder artifact but provide data only to lower spatial resolution (Kučerka et al., 2005). Models for the electron density profile are employed, and the best fit to the data give values of the structural parameters. The lipid molecular volume is also obtained and used to constrain the fitting of the models.

Materials and Methods

Synthetic DOPC (di18:1PC; lot 18:1PC-177), POPC (16:0,18:1PC; lots 16:0–18:1PC-LAM10, -116, -154) and di22:1PC (dierucoylphosphatidylcholine; lot 22:1PC-33) were purchased from Avanti Polar Lipids (Alabaster, AL) and used without further purification. Two lots of POPC that differed in the extent of acyl chain migration (< 5% and 25%) were studied using X-ray methods. Thin-layer chromatography (TLC) was used as previously described (Tristram-Nagle et al., 2002) to assess lipid damage before and after the Cornell High Energy Synchrotron Source (CHESS) experiment.

ORIENTED SAMPLES

Oriented stacks of approximately 1,500 bilayers were prepared using the rock-and-roll method (Tristram-Nagle et al., 1993); 4 mg of lipid in a chloroform:trifluoroethanol mixture (1:1, v:v) was deposited onto a flat $15 \times 30 \times 1$ mm Si wafer and subjected to

shear during evaporation of the organic solvent. The samples were trimmed to a strip that occupied only the central 5 mm of the 15 mm width of the substrate. Translating along the 30 mm length of the sample (x direction), which is perpendicular to the y direction of the beam, provides many fresh spots for taking X-ray data and avoiding radiation damage. TLC revealed that the damage caused by synchrotron radiation was negligible for these samples.

ULVs

Lipid (10 mg) was mixed with 500 μ l water (Barnstead nanopure) in a sealed nalgene tube. Extruded ULVs were prepared from a multilamellar dispersion using the Avanti miniextruder as described previously (Kučerka et al., 2005). The sample was filled into a circular lumen 1.5 mm thick in the beam direction. The time between sample preparation and measurement was about 10 h. Absence of any oligolamellar distortions to the resulting form factor indicated that the vesicles were unilamellar. Small-angle neutron scattering from similarly prepared samples that extended to small enough angle to resolve the vesicular form factor obtained a mean unilamellar diameter of 600 Å (Kučerka, Kiselev & Balgavý, 2004a).

X-RAY SCATTERING

X-ray data were taken on two separate trips to the D-1 station of CHESS with similar but not identical setups. X-rays of wavelength ($\lambda = 1.172$ Å, 1.1808 Å) were selected using multilayer monochromators (Osmic, Detroit, MI; Advanced Photon Source, Chicago, IL), which had 1.2% and 1.5% full-width half-maximal (FWHM) energy dispersion, respectively. The beam for oriented samples was narrow (0.28 mm) to provide small angular divergence (1.4×10^{-4} radian) in the horizontal direction, which is essential for analysis of diffuse scattering. The beam was 1.2 mm tall to ensure that all of the sample (5 mm along the beam) was in the footprint of the beam for all rotation angles θ that extended up to 5° ($q_z = 0.93$ Å $^{-1}$). Exposures were typically 120 s, during which time the sample was continuously rotated from -3° to $+7^\circ$ at constant angular speed to ensure that the intensity was uniformly collected for all q values in the range where sample scattering was detectable. The beam for the ULV samples was 0.28×0.28 mm square. For both oriented stacks and ULV samples, total exposure time on a sample spot was limited to 4 min, during which time the scattering remained constant. Data were collected using a Medoptics charge-coupled device (CCD) with a $1,024 \times 1,024$ pixel array, each pixel having average linear dimension, 47.19 μ m. The CCD to sample distance was $s = 248.2$ mm for oriented samples and $s = 347.8$ mm for ULV samples, calibrated using a silver behenate standard. Collected images were dezingered and processed for CCD distortion and intensity corrections (Barna et al., 1999), using calibrated files supplied by CHESS, and dark CCD levels were subtracted. Background subtraction employed images of the scattering from the bare substrate for oriented samples and images of the scattering from water in the ULV cell. These images were normalized to the data images using the transmitted beam intensity, which was recorded on all CCD images after attenuation by a factor of 1.6×10^7 by a 225- μ m-thick molybdenum semitransparent beam stop.

LIPID VOLUMES

The volume per lipid molecule (V_L) was obtained by neutral density flotation for POPC in mixtures of D₂O and H₂O, and our value agrees well with that of Hianik et al. (1998). Because di22:1PC floated in pure H₂O, its partial specific volume was first obtained as a function of mole fraction from a sequence of mixtures of

di22:1PC in POPC up to the mole ratio of 0.33 di22:1PC/POPC at which the mixture was neutrally buoyant in pure H₂O. The partial specific volume was constant as a function of mole fraction, as would be expected for two similar lipids well into the fluid phase. (The transition temperatures are −17°C and 13°C, respectively, for DOPC and di22:1PC [Lewis, Sykes & McElhane, 1988] and −5°C for POPC [Perly, Smith & Jarrell, 1985].) The partial specific volume of di22:1PC was then taken as its volume in the pure di22:1PC bilayer. This value agreed very well with that calculated using a recently proposed formula that was empirically derived from the volumes of a variety of unsaturated lipids (Koenig & Gawrisch, 2005).

Results

PRIMARY X-RAY DATA

Figure 1 shows a background-subtracted CCD image of a ULV sample of di22:1PC at 30°C. Compared to the background, the scattering intensity from the lipid only (data minus background) is very strong and robust in the first lobe and second lobe up to $q_z = 0.30 \text{ \AA}^{-1}$, but it is weaker than the intensity from the background for larger q_z . Even though Figure 1 clearly indicates a third lobe, not all of the third lobe data are used in the analysis because of the delicate subtraction of the background. For this sample and DOPC, only data for $q_z < 0.4 \text{ \AA}^{-1}$ were used and for $q_z < 0.5 \text{ \AA}^{-1}$ for POPC, with estimated errors for each q region assigned proportional to the smoothness of the nearby data points.

Figure 2 shows a background-subtracted CCD image of an oriented sample of di22:1PC at 30°C. The repeat spacing (D) was determined from the locations of the attenuated direct beam and the $h = 1, 2, 3$ and 4 orders. On the meridian ($q_r = 0$), there are sharp minima in the intensity near $q_z = 0.22, 0.35, 0.52$ and 0.63 \AA^{-1} .

ANALYSIS OF DATA TO OBTAIN $F(q_z)$

The bilayer form factor (sometimes called the structure factor) $F(q_z)$ is the Fourier transform of the minus fluid electron density profile $\rho(z) - \rho_w$ normal to the bilayer, where ρ_w is the electron density of water.

ULVS

Relative values of $|F(q_z)|$ are obtained routinely from the background-subtracted intensities $I(\mathbf{q})$ of ULV samples:

$$I(\mathbf{q}) = |F(q_z)|^2/q_z^2 \quad (1)$$

This is the appropriate relation for a sample in which each vesicle scatters independently of neighboring vesicles and for q values large enough ($> 0.01 \text{ \AA}^{-1}$) that modulation of $I(\mathbf{q})$ due to the finite size of the

vesicle is negligible (Kučerka et al., 2004b) and small enough that q_z^{-2} is a good approximation to the Lorentz factor. Figure 3 shows results on an absolute vertical scale which is obtained in the subsequent analysis.

Multilamellar Vesicles

Conventional data for multilamellar samples were obtained from the integrated intensities of the intense diffraction peaks, which occur only at discrete values of $q_h = 2\pi h/D$. Fluctuations in the noncrystalline samples smear these peaks, but application of liquid crystallography and precise measurements of the peak shapes enabled the ratios of peak intensities to be obtained for the lower orders of diffraction (Nagle et al., 1996). Figure 3 shows these older results for the first two orders of DOPC for seven different D spacings (Tristram-Nagle, Petrache & Nagle, 1998). A common scaling factor for the $h = 1$ and $h = 2$ orders was chosen in the subsequent modeling for each D spacing, so there are only seven independent data.

The ULV data for DOPC in the first lobe are in excellent agreement with these older multilamellar vesicle (MLV) data, so we have not taken MLV data for other lipid bilayers because the experiments are relatively more difficult and the ULV data are more plentiful.

Oriented Stacks

These samples are multilamellar, like the MLVs, but the primary data that we use are diffuse data, like the ULVs. The scattering intensities $I(\mathbf{q})$ are first corrected for differential absorption at different scattering angles due to different path lengths in the sample (Tristram-Nagle et al., 2002). Then, the scattering intensity for a stack of oriented bilayers is the product:

$$I(\mathbf{q}) = S(\mathbf{q})|F(q_z)|^2/q_z^2 \quad (2)$$

where $\mathbf{q} = (q_r, q_z)$, $S(\mathbf{q})$ is the structure factor, $F(q_z)$ is the bilayer form factor and q_z^{-1} is the usual low-angle approximation to the Lorentz factor for oriented samples. To obtain $|F(q_z)|^2$ from the measured $I(\mathbf{q})$, we first obtain $S(\mathbf{q})$, which may be thought of as an interference factor. Unlike crystalline samples, $S(\mathbf{q})$ is not composed of simple delta functions that give sharp Bragg peaks at discrete values of \mathbf{q} . Instead, $S(\mathbf{q})$ allows non-zero diffuse scattering for continuous ranges of \mathbf{q} . We then essentially divide $S(\mathbf{q})/q_z$ into $I(\mathbf{q})$ to obtain $|F(q_z)|$.

Our method for obtaining $S(\mathbf{q})$ has been recently developed and applied to DOPC (Lyatskaya et al., 2001; Liu & Nagle, 2004) as well as DLPC and DMPC (Chu et al., 2005; Kučerka et al., 2005). This method is based on the theory of smectic liquid

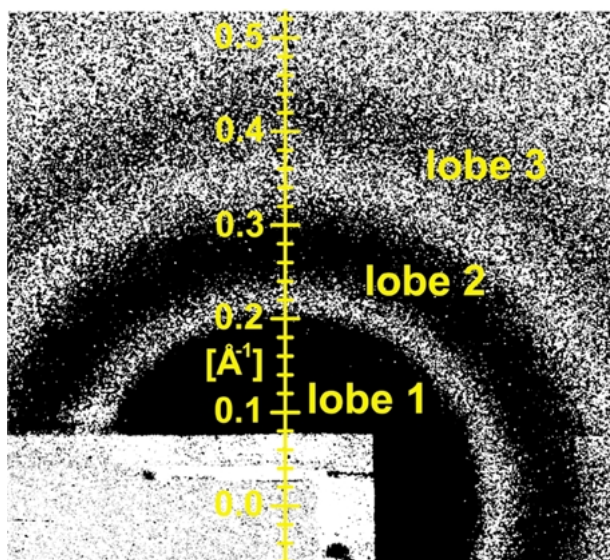


Fig. 1. (Color online) Gray-scale plot of the log of the intensity from a sample of ULVs of di22:1PC at 30°C with the water background-subtracted. The intensity is greatest in the dark regions, labeled as lobes 1–3. The lobes are separated by light regions of low intensity within which there are zero intensities near $q_z = 0.22$ and $q_z = 0.35 \text{ \AA}^{-1}$. The scale is for q_z in \AA^{-1} . The rectangular light region at the lower left is the shadow of a rectangular beamstop.

crystals, which have two primary parameters, the bilayer bending modulus (K_C) and the compression modulus (B). The numerical values of these two material parameters are determined by fitting the theory to the data, as shown in Figure 4 for a few of the ≈ 250 values of q_z that were fitted. The overall quality of the fits for the many (75,000) data points indicates that the theory works.

Table 1 gives the fully hydrated D spacings that were obtained from MLV samples in excess water. Some of our oriented samples had D spacings that were the same as the fully hydrated values for DOPC and POPC, whereas our most hydrated oriented sample of di22:1PC had a slightly smaller D spacing of 69.2 Å (Fig. 2). We also varied the hydration of the samples to include D values smaller than the fully hydrated values. Just as for DMPC (Chu et al., 2005) and as expected by theory, the results for K_C were statistically constant as a function of D ; the mean values for each lipid are shown in Table I. In strong contrast, the values of the B compression modulus increase exponentially as D decreases, similar to our results for DMPC. This $B(D)$ dependence is important for studying interactions between bilayers; that topic will be treated in a different report.

The results for $|F(q)|$, corrected for undulations (Nagle & Tristram-Nagle, 2000), are shown in Figure 3 for oriented samples of the three lipids. Only one scaling factor, determined by the subsequent modeling, is used for all the $|F(q)|$ from each sample.

The results for DOPC include the results reported previously from one sample with $D = 63.2 \text{ \AA}$ (Liu & Nagle, 2004) and results from one additional new sample with $D = 62.6 \text{ \AA}$; these results are essentially the same, consistent with the structure staying the same until much smaller D spacings, so the same symbols are used in Figure 3. Results for POPC and di22:1PC are all new.

For q smaller than $4\pi/D$, where the $h = 2$ order peak occurs, the diffuse scattering from oriented stacks becomes weak compared to the peak scattering, so the $|F(q)|$ values from oriented stacks are not reliable and are not shown in Figure 3. Similarly, $|F(q)|$ results cannot be obtained by this method when the D spacing decreases too much, typically by more than 5 Å below the fully hydrated D because bilayer undulations are suppressed by strong interbilayer interactions and there is insufficient diffuse scattering for analysis. For small q , the $|F(q)|$ results from ULVs are distinctly superior to the results from diffuse scattering from oriented stacks. For large q , in contrast, the scattering from ULVs is much weaker than background while the diffuse scattering from oriented stacks remains strong enough for analysis. The $|F(q)|$ results from oriented samples overlap nicely with the ULV results for values of q greater than $4\pi/D$. Our subsequent analysis therefore uses the best of both kinds of data.

QUANTITATIVE BILAYER STRUCTURE

To obtain bilayer structure, it is important to use, in addition to the basic X-ray results for $F(q_z)$, any additional information, such as the measured volume V_L and the numbers of electrons on the component groups of the lipid. All such information can be accommodated by using a model of the electron density that can then be fit to $F(q_z)$. Our previous analysis employed a model of electron density composed of gaussians for the localized phosphatidylcholine (PC) and the carbonyl-glycerol (CG) in the headgroups and another negative gaussian to account for the methyl trough. These are superimposed on a smooth baseline function that represents the hydrocarbon plateau, the aqueous plateau and a smooth transition between them (Wiener, Suter & Nagle, 1989). We now call this the hybrid baseline (HB) model. Figure 5 shows graphically the different components that comprise the HB model. We have recently defined a second model that we call the H2 model (Klauda et al., 2005) because it also involves a hybridization, but the baseline function in the HB model is eliminated in favor of a more straightforward and more detailed representation of the methylene plateau and the water plateau. Figure 6 shows graphically the different components that comprise the H2 model. For both models, the electron density of the double-bonded moiety is averaged with the

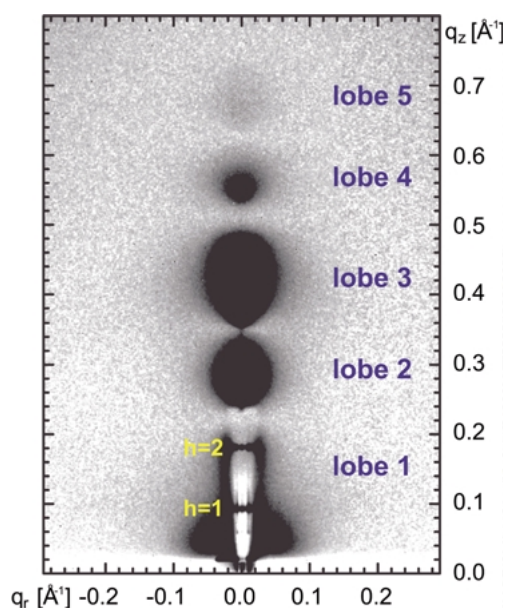


Fig. 2. (Color online) Gray-scale plot of the log of the intensity from an oriented stack sample of di22:1PC ($D = 69.2 \text{ \AA}$) at 30°C . Black is most intense. Orders $h = 1$ and $h = 2$ were attenuated by a factor of 1,600 by a 100- μm -thick vertical molybdenum finger on the beamstop to prevent overexposure of the CCD. The gray scale emphasizes the lobes of diffuse scattering, which are demarcated by zeros in the intensity where the form factors change sign. The narrow line of intensity along the $q_r = 0$ meridian which is apparent between lobes 2 and 3 is specular reflectivity from the silicon substrate. The light region at the bottom is the shadow of a wide beamstop.

methylene plateau because their electron densities differ by less than 10% so that a separate gaussian feature for the double bonds makes a negligible difference in $F(q_z)$. Tests of the two models using molecular dynamics simulations have shown that, when the information that is available experimentally is provided to programs that fit the models, both provide acceptable agreement with the complete information available from the simulations (Klauda et al., 2005). The advantage of using different models is to provide an estimate of the uncertainty that is inherent in having to choose the functional form of the model. Uncertainties in A from uncertainties in constrained parameters in the modeling are estimated as 0.5 \AA^2 (Klauda et al., 2005).

Even with all the constraints that are imposed on the models from outside information, both models fit the $|F(q_z)|$ data very well. Figure 3 shows the fits for the HB model. The fit for the H2 model is visually indistinguishable. The main structural parameters that provide these fits are given in Table 1. These parameters are illustrated graphically in Figure 5, which shows the electron density profiles that are obtained from the fit for the HB model and in Figure 6 for the H2 model. Despite the considerable differences between the HB and H2 models in how the contributions of the different molecular compo-

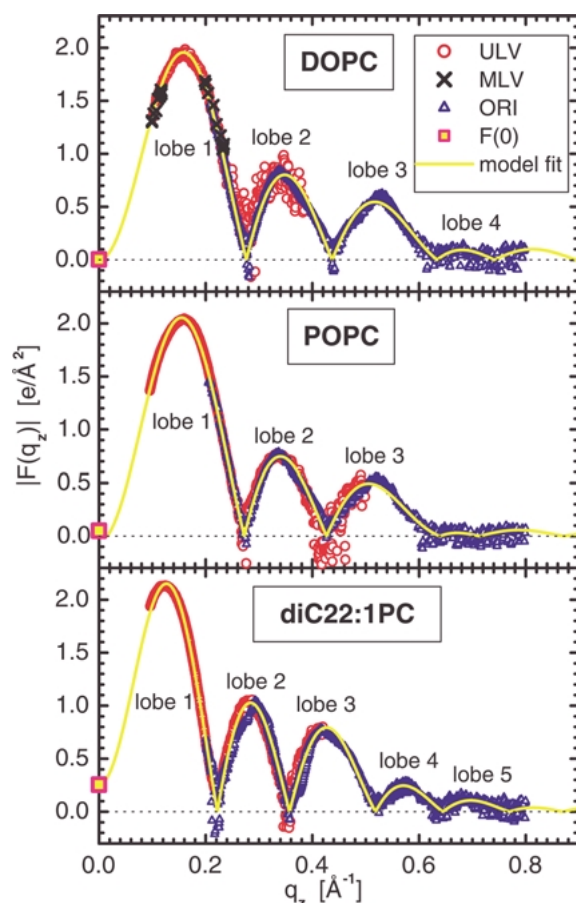


Fig. 3. (Color online) Absolute values of the form factors $F(q_z)$ at $T = 30^\circ\text{C}$ on an absolute scale for DOPC, POPC and di22:1PC. Data are from ULV samples (*open circles*), MLV samples (*X*, DOPC only), oriented samples (*triangles*) and $F(0)$ (*squares* at $q_z = 0$) from volume measurements. Negative values of $|F(q_z)|$ indicate statistical fluctuations where scattering intensity is weak. The lines show the fits obtained by the structural analysis, which provides the relative scale factors for the different data sets.

nents are made, the total electron densities are quite similar when plotted on the same graph (*not shown*), which is consistent with the agreement of the two model $|F(q_z)|$ results.

Discussion

Comparison of the results in Table 1 illuminates similarities in lipid structure as well as differences due to differences in chain length and unsaturation. To enhance this discussion, we have added our recent results for DMPC (Kučerka et al., 2005), which were also obtained at 30°C .

VOLUMES

The volumes (V_L) of the four lipids differ considerably. Assuming that the volume of the headgroup (V_H) is constant because it is immersed in water, the

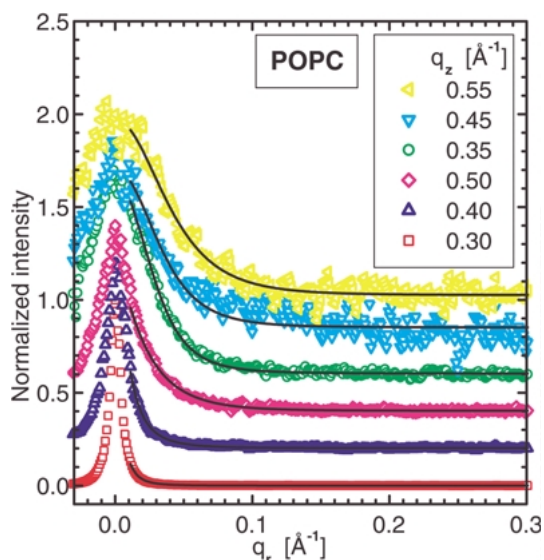


Fig. 4. (Color online) The POPC scattering intensities along horizontal trajectories in CCD images, such as those in Figure 2, are shown by symbols. These trajectories are essentially along varying q_r . The different symbols distinguish different slices, essentially different values of q_z . To facilitate viewing the wide range of values, each curve has been normalized to unity at its maximum value and the curves are offset vertically. The noisier curves have smaller intensity because their q_r values are close to the zeros in $F(q_z)$. The solid lines show the fit of the smectic liquid crystal theory simultaneously to all the data, with one scaling parameter for each q_r that is closely related to $|F(q_z)|$. Fitting was performed only for $q_r > 0.01 \text{ \AA}^{-1}$ to avoid artifacts from specular reflectivity.

$V_H = 331 \text{ \AA}^3$ that was obtained for the DMPC gel phase (Tristram-Nagle et al., 2002) is subtracted from V_L to obtain the volume of the hydrocarbon chains (V_C), which is further partitioned into the volume V_{CH_3} of each terminal methyl, the volume V_{CH_2} of each methylene and the volume $V_{HC=CH}$ of the double-bonded moiety. The terminal methyls have a larger volume than the methylenes by a ratio V_{CH_3}/V_{CH_2} that many studies (Nagle & Wiener, 1988; Wiener & White, 1992; Armen, Uitto & Feller, 1998), including this one, put in the range 1.9–2.0. The ratio $V_{HC=CH}/V_{CH_2}$ has been predicted to be 1.60 from both molecular dynamics (MD) simulations (Armen et al., 1998) and from recent volumetric studies of many unsaturated lipids (Koenig & Gawrisch, 2005). Using V_C and these ratios, the individual component volumes are obtained as shown in Table 1. These component volumes are essentially the same for all four lipids. We conclude that the differences in lipid volumes of phosphatidylcholine lipids are primarily due to differences in the number of carbons in the hydrocarbon chains. This is not surprising because all these lipids are in the disordered fluid phase at the same temperature.

AREAS

In contrast to the volumes, the areas per lipid molecule (A) vary significantly for the four lipids in

Table 1. Structural results

	DOPC	POPC	di22:1PC	DMPC
D_{FH} (Å)	63.2	64.0	70.0	62.7
K_c (10^{-13} erg)	8.0	8.5	12.7	6.9
V_L (\AA^3)	1,303	1,256	1,522	1,101
$V_{HC=CH}$ (\AA^3)	44.4	44.2	44.2	–
V_{CH_2} (\AA^3)	27.7	27.6	27.6	27.7
V_{CH_3} (\AA^3)	53.3	53.6	53.6	52.6
A (\AA^2)	72.4	68.3	69.3	60.6
$2D_c$ (Å)	26.8	27.1	34.4	25.4
D_{HH} (Å)	36.7	37.0	44.3	35.3
$2z_{PC}$ (Å)	37.4	38.2	45.4	35.5
$2z_P$ (Å)	37.2	37.6	45.0	35.6
$2z_{CG}$ (Å)	29.4	29.8	37.2	27.8
D_B (Å)	44.8	45.1	52.4	43.4
D_B (Å)	36.0	36.8	44.0	36.3
n_W	32.8	31.0	30.0	26.6
n'_W	10.7	9.4	9.7	7.2
σ_{PC} (Å)	2.29	2.70	2.57	2.21
σ_{CG} (Å)	2.14	2.43	2.40	1.90
σ_M (Å)	2.92	2.95	3.66	2.23

See text for definitions of symbols.

Table 1. The small DMPC area cannot be explained by the smaller number of 14 carbons in the hydrocarbon chains. Dilauroylphosphatidylcholine (DLPC), with only 12 carbons per chain, has a larger area, $A_{DLPC} = 63.2 \text{ \AA}^2$ (Kučerka et al., 2005). Dipalmitoylphosphatidylcholine (DPPC), with 16 carbons per chain, has a larger area, 64 \AA^2 (Nagle & Tristram-Nagle, 2000), but that is for $T = 50^\circ\text{C}$. A better perspective is obtained by estimating the area that DPPC would have at $T = 30^\circ\text{C}$ if it did not undergo transitions into chain-ordered phases; an areal thermal coefficient of expansion of $0.004/\text{degree}$ (Needham & Evans, 1988) is applied to obtain $A_{DPPC} = 59 \text{ \AA}^2$ extrapolated to 30°C . As has also been concluded from neutron scattering studies of ULVs (Balgavý et al., 2001), increasing chain length decreases A for saturated lipids at the same temperature. Similarly to saturated lipids, increasing chain length in di-monounsaturated lipids also decreases A by roughly the same amount, as shown in Figure 7. Our results are also shown in Figure 8, where they are compared to two previous results. While there are differences for the values of A , all studies agree on the slopes that give the changes with chain length. By explicitly displaying the chain-length dependence, Figure 7 emphasizes that adding a double bond to both hydrocarbon chain increases A by about 14.5 \AA^2 .

The most remarkable result in Table 1 is that the area of POPC is considerably closer to the area of DOPC than it is to DMPC, suggesting that the effect on bilayer structure of replacing saturated lipids by a lipid with a double bond on one chain is much greater than the additional effect of putting a double bond on both chains. Figure 7 allows this idea to be more

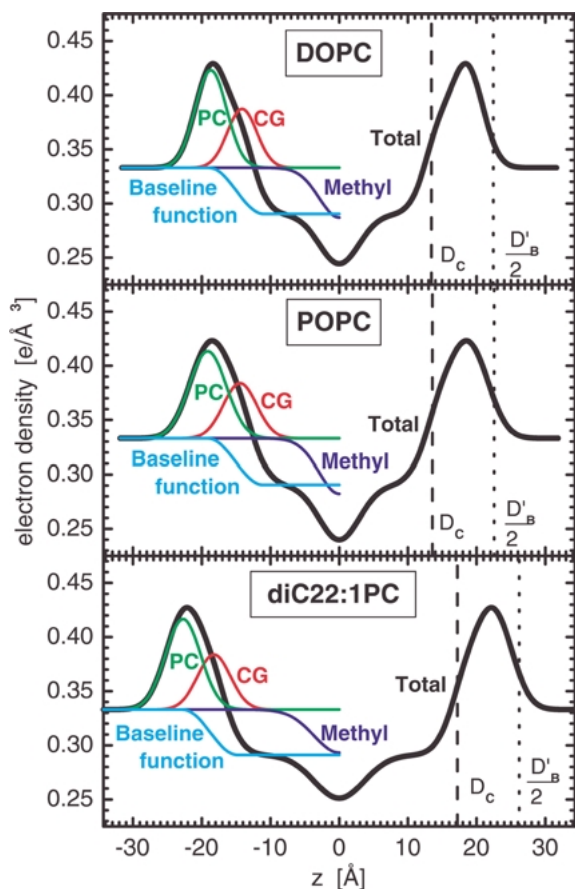


Fig. 5. (Color online) The *thick lines* show the total electron density profiles for DOPC, POPC and di22:1PC obtained by fitting the HB electron density model to the form factor data in Figure 3. The individual contributions to the total electron density of the phosphatidylcholine PC component, the carbonyl-glycerol CG component, the terminal methyl component and the baseline function are shown by *thin lines* as noted on the left side of the figure. On the right side of the figure are shown the Gibbs dividing surface for the hydrocarbon region D_C (*dashed vertical lines*) and the steric boundary $D'_B/2$ (*dotted vertical lines*).

precisely quantified because complications due to the chain-length dependence are explicitly displayed. A measure of the effect of the first double bond is then the fraction f of the increase from the $m = 0$ line to the $m = 1$ line along a constant n line. Our result for A_{POPC} gives $f_{\text{POPC}} = 0.68$, suggesting that about two-thirds of the area increase comes from putting a double bond on one chain, twice as much as adding a double bond to the second chain.

Figure 7 also compares earlier results. Pabst et al. (2000) reported A_{POPC} was only 54 \AA^2 at $T = 2^\circ\text{C}$ and 64 \AA^2 at $T = 50^\circ\text{C}$. Interpolation to $T = 30^\circ\text{C}$ gives $A \approx 59 \text{ \AA}^2$, considerably smaller than our value in Table 1, and the unlikely result that the effect of one double bond is only $f_{\text{POPC}} = 0.08$. Those earlier results were also based on diffuse scattering but from unoriented MLVs for which the $|F(q_z)|$ data only extended to 0.5 \AA^{-1} , thereby requiring a less realistic

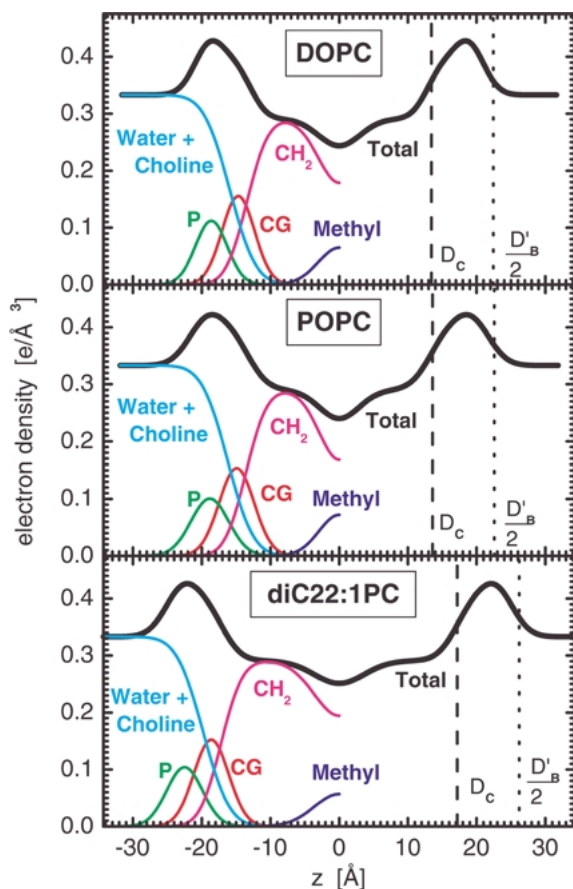


Fig. 6. (Color online) The *thick lines* show the total electron density profiles for DOPC, POPC and di22:1PC obtained by fitting the H2 electron density model to the form factor data in Figure 3. The individual contributions to the total electron density of the phosphate P component, the carbonyl-glycerol CG component, the terminal methyl component, the methylene component and the water-choline component are shown by *thin lines* as noted on the left side of the figure. On the right side of the figure are shown the Gibbs dividing surface for the hydrocarbon region D_C (*dashed vertical lines*) and the steric boundary $D'_B/2$ (*dotted vertical lines*).

bilayer model consisting of only a headgroup gaussian and a terminal methyl gaussian. A more plausible $f_{\text{SOPC}} = 0.30$ is obtained from the $A = 61.4 \text{ \AA}^2$ reported for stearylloleoylphosphatidylcholine (SOPC) by Koenig et al. (1997), who used the gravimetric method. In the same report, $A_{\text{DMPC}} = 59.5 \text{ \AA}^2$ was reported, only 1.2 \AA^2 less than our current value. If we add this difference to their A_{SOPC} , their f_{SOPC} increases to 0.38, but this is still considerably smaller than our value for POPC and would reverse our conclusion regarding the relative effect of the first and second double-bonded chains. Another comparison involving Egg phosphatidylcholine (EggPC) is also shown in Figure 7, where $A_{\text{EggPC}} = 69.5 \text{ \AA}^2$ (Petrache, Tristram-Nagle & Nagle, 1998; Rand & Parsegian, 1989) gives an area proportionality of 0.77. EggPC is a mixture of lipids with chains of different lengths and numbers of double bonds, with compo-

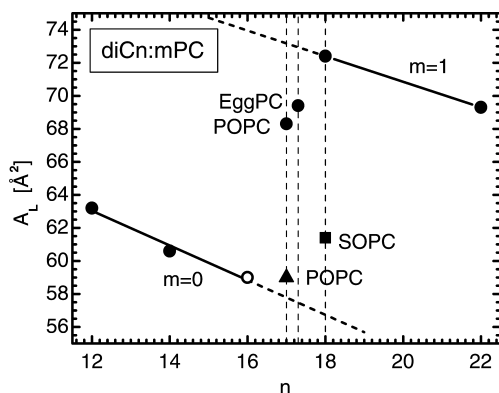


Fig. 7. Area A per lipid as a function of chain length n for different numbers m of double bonds per chain at 30°C . Saturated lipids have $m = 0$, di-monounsaturated lipids have $m = 1$ and POPC and SOPC have $m = 0.5$. *Solid circles* show results from this lab, the *open circle* for DPPC is extrapolated from $T = 50^\circ\text{C}$, the *triangle* for POPC is interpolated from Pabst et al. (2000) and the *square* for SOPC is from Koenig, Strey and Gawrisch (1997).

sition determined by Avanti Polar Lipids as $0.34(16:0) + 0.02(16:1) + 0.11(18:0) + 0.32(18:1) + 0.18(18:2) + 0.03(20:4)$ for an average chain length $n = 17.3$ and an average number of double bonds per chain of 0.80. If it is assumed that each double bond has the same effect on A , then the area proportionality of 0.77, when normalized to one double bond per lipid, suggests $f_{\text{EggPC}} = 0.48$. However, chains with additional double bonds are not likely to affect A as much as the first double bond, so an alternative comparison is to calculate $m = 0.55$ as the fraction of chains with any double bonds. When normalized to one double bond per lipid, this suggests that $f_{\text{EggPC}} = 0.77 \cdot (0.50/0.55) = 0.70$, in good agreement with our value for POPC. A final perspective can be obtained from a nuclear magnetic resonance (NMR) study (Seelig & Seelig, 1977) that shows that the order parameter of the *sn*-1 palmitic chain is smaller for POPC than for DPPC and that estimates the effective length of this chain to be 12.8 \AA for POPC and 13.7 \AA for DPPC at 42°C , at which temperature A_{DPPC} can be extrapolated to be 62 \AA^2 or 31 \AA^2 per chain. Let us make the assumption that the areas of the palmitic chain are inversely proportional to their lengths, so its area in POPC is estimated as $31 \cdot (13.7/12.8) = 33.2 \text{ \AA}^2$ at 42°C , which extrapolates to 31.6 \AA^2 at 30°C . Now add the area of an oleoyl chain 36.2 \AA^2 from DOPC to obtain an estimated area of 67.8 \AA^2 for POPC at 30°C , which is close to our result.

Nevertheless, we were surprised that our A for POPC is as large as we report, and we therefore scrutinized our results for POPC carefully. Exactly the same methodology was employed as for the di22:1PC samples that give plausible results compared to others in the literature, as seen in Figure 8 and for our earlier studies on DMPC and DOPC.

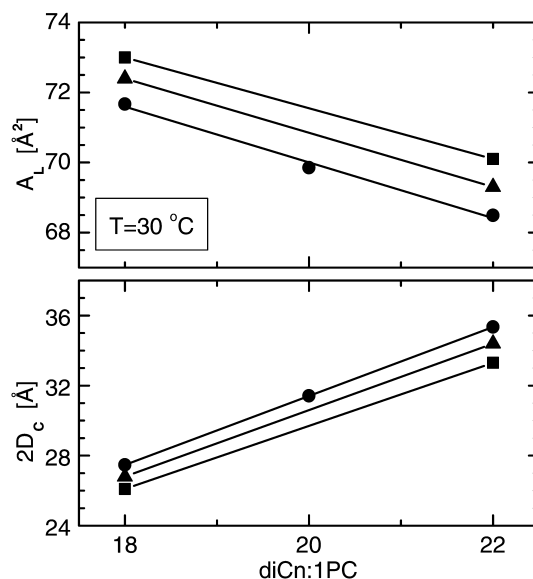


Fig. 8. Results for A per lipid and the hydrophobic thickness $2D_C$ as a function of chain length for di-monounsaturated lipids at 30°C . *Triangles* show this work; *circles* are for neutron scattering from ULVs (Kučerka et al., 2004c) analyzed following the method of Kučerka et al. (2004b). *Squares* are from results of Lewis and Engelman (1983) extrapolated from data taken at lower temperatures using a coefficient of areal expansion of 0.0042 per degree and a coefficient of linear expansion of -0.0033 per degree.

One concern for POPC is acyl chain migration that results in a mixture of POPC and oleoylstearylphosphatidylcholine (OPPC); one of our samples had 25% migration and another had 5%. Our results for material properties were the same for these two samples, which is consistent with Rawicz et al. (2000) who reported the same K_C values for SOPC and OPPC. Also, one of our POPC samples had 2–5% lysolecithin as determined by TLC, and it had a slightly smaller volume ($1,250\text{--}1,255 \text{ \AA}^3/\text{lipid}$). Variations in the area that we obtained from these samples were at the level of $\pm 1.0 \text{ \AA}^2$.

THICKNESSES

Table 1 reports several different thicknesses for these bilayers. The most important thickness for considering hydrophobic matching of proteins in lipid bilayers is the hydrocarbon thickness, $2D_C$, which is closely related to the area through $D_C = V_C/A$. Table I shows the expected result that the hydrophobic region is much thicker for di22:1PC with many more carbons per chain. Although DMPC chains have fewer carbons, $2D_C$ is nearly as thick as for DOPC and POPC because A is considerably smaller for DMPC and the chains are forced to travel further, on a per carbon basis, from the headgroups into the bilayer interior in order to conserve volume. Similarly, POPC and DOPC have nearly the same value of $2D_C$. The smaller A for POPC suggests that

the palmitoyl chain in POPC has a smaller area than its corresponding oleoyl chain in DOPC. Again, on a per carbon basis, the palmitoyl chain would then be more stretched toward the bilayer center, but it would still have the same value of D_C because there are two fewer carbons.

The most obvious thickness that emerges from X-ray studies is the distance D_{HH} between the maxima in the electron density profile. This is often equated in the literature to the distance between the electron-dense phosphate peaks. In the H2 model, this latter distance is the distance $2z_P$ between the P gaussians that represent only the phosphate group, whereas in the HB model it is $2z_{PC}$ between the PC gaussians, which also include the cholines. The differences $z_{PC} - z_P$, though small and statistically noisy, when averaged over the four lipids in Table I, are consistent with the PC dipole being tilted somewhat upward into the aqueous phase compared to being completely parallel to the bilayer surface. Also, as shown by Table I and reported earlier (Kučerka et al., 2005), D_{HH} is only 0.2 Å smaller than $2z_{PC}$ for DMPC. However, for the unsaturated lipids, Table I shows that both the differences $2z_{PC} - D_{HH} \approx 1$ Å and $2z_P - D_{HH} \approx 0.6$ Å are somewhat larger. To explain this, we first note that the position $D_{HH}/2$ of the maximum is determined by the sum of all the component groups. As is well known, adding a smaller gaussian, such as the CG gaussian, to a larger one shifts the position of the maximum from the center of the larger gaussian toward the smaller one, and this shift increases as the widths of the gaussians increase. Focusing just on the most electron-dense phosphate group located at z_{PC} and the next most electron-dense carbonyl-glycerol groups located at $z_{CG} < z_{PC}$, one expects that $2z_{PC} - D_{HH}$ is positive. Furthermore, one expects this difference to increase for the unsaturated lipids because they are more disordered and should therefore have larger widths of their distribution functions, an expectation that is indeed confirmed by the fits shown by the values of σ_{PC} and σ_{CG} in Table I.

Another important thickness for interactions of bilayers with other bilayers or with macromolecules is the steric thickness, D'_B . We calculate this by assuming a thickness of 9 Å for each of the two headgroup regions, i.e., $D'_B = 2D_C + 18$ Å. This convention is consistent with a nearly complete decay of the electron density to that of pure water, as seen in Figures 5 and 6. The last thickness in Table I is the Luzzati thickness, $D_B = V_L/A$, which is the Gibbs dividing surface between water and the bilayer. Its complement, $D_W = D - D_B$, is the effective thickness of the water, treated as a uniform slab, that plays a role in the compressibility correction to the area when osmotic pressure is applied (Rand & Parsegian, 1989; see equation 2 in Nagle & Tristram-Nagle, 2000).

WATER AND WIDTHS

Table I reports the number n_W of water molecules per lipid in the multilamellar samples; this is a pertinent number for setting up computer simulations. The number of waters is further broken down into the number n'_W that are included in the interfacial headgroup zone that we have taken to be 9 Å thick. Variations in n'_W with the different lipids are directly related to the area by $n'_W = (A \cdot 9 \text{ Å} - V_H)/V_W$.

Finally, Table I gives the widths of the gaussian distributions, σ_M for the methyl trough, σ_{PC} for the phosphate-choline group and σ_{CG} for the carbonyl-glycerol group that were obtained from fitting the data. The first general trend exhibited is that the CG component has the smallest width. This is plausible because the hydrophobic interaction with water can be thought of as a surface tension that favors planarity and suppresses fluctuations in the positions of this component. This result is also consistent with, but not compelled by, the NMR result that the dynamical time constant is largest for this region of the lipid molecule (Finer, Flook & Hauser, 1972). In contrast, conformational degrees of freedom between the glycerol and the phosphate might allow the phosphate group to sample a wider range of z levels and still be solvated by the n'_W water molecules in the headgroup region. The second general trend is that all the widths are significantly smaller for DMPC. This can be rationalized by the general argument that the smaller A for DMPC requires it to be more ordered. The third trend is that σ_M is largest for di22:1PC and smallest for DMPC. The location of the terminal methyl on a chain can be thought of as the end of a somewhat random walk starting at the headgroup surface. The fact that a distribution of end points on a random walk grows with the number of steps qualitatively explains the larger σ_M for di22:1PC with its greater number of carbons and the smaller σ_M for DMPC.

Synchrotron X-ray beamtime was provided by CHESS (National Science Foundation grant DMR-0225180). We thank Hee Kyoung Ko for her help with the data collection at CHESS and Alex Greenwood, a student in the Howard Hughes Summer Undergraduate Research Program, for his help in determining lipid volumes using density centrifugation. This research was supported by National Institutes of Health grant GM44976 (to J. F. N.).

References

- Armen, R.S., Uitto, O.D., Feller, S.E. 1998. Phospholipid component volumes: Determination and application to bilayer structure calculations. *Biophys. J.* **75**:734–744
- Balgavý, P., Dubničková, M., Kučerka, N., Kiselev, M.A., Yaradaikin, S.P., Uhríková, D. 2001. Bilayer thickness and lipid interface area in unilamellar extruded 1,2-diacylphosphatidylcholine liposomes: A small-angle neutron scattering study. *Biochim. Biophys. Acta* **1512**:40–52

- Barna, S.L., Tate, M.W., Gruner, S.M., Eikenberry, E.F. 1999. Calibration procedures for charge-coupled X-ray detectors. *Rev. Sci. Instrum.* **70**:2927
- Chu N., Kučerka, N., Liu, Y., Tristram-Nagle, S., Nagle, J.F. 2005. Anomalous swelling of lipid bilayer stacks is caused by softening of the bilayer modulus. *Phys. Rev. E* **71**:041904 (1–8)
- Eldho, N.V., Feller, S.E., Tristram-Nagle, S., Polozov, I.V., Gawrisch, K. 2003. Polyunsaturated docosahexaenoic vs docosapentaenoic acid - differences in lipid matrix properties from the loss of one double bond. *J. Am. Chem. Soc.* **125**:6409–6421
- Finer, E.G., Flook, A.G., Hauser, H. 1972. Mechanism of sonication of aqueous egg yolk lecithin dispersions and nature of the resultant particles. *Biochim. Biophys. Acta* **260**:49–58
- Gennis, R.B. 1989. Biomembranes. Molecular Structure and Function. Springer-Verlag, New York
- Hanahan, D.J. 1997. A Guide to Phospholipid Chemistry. Oxford University Press, New York, pp 65–66
- Hianik, T., Haburcák, M., Lohner, K., Prenner, E., Paltauf, F., Hermetter, A. 1998. Compressibility and density of lipid bilayers composed of polyunsaturated phospholipids and cholesterol. *Colloids Surf A Physicochem Eng Aspects* **139**: 189–197
- Klauda J.B., Brooks B.R., Pastor R.W., Kučerka N., Nagle J.F. 2005. A simulation-based model for interpreting X-ray data from lipid bilayers. *Biophys. J.* (in press)
- Koenig B.W., Gawrisch K. 2005. Specific volumes of unsaturated phosphatidylcholines in the liquid crystalline lamellar phase. *Biochem. Biophys. Acta* **1715**:65–70
- Koenig, B.W., Strey, H.H., Gawrisch, K. 1997. Membrane lateral compressibility determined by NMR and X-ray diffraction: Effect of acyl chain polyunsaturation. *Biophys. J.* **73**:1954–1966
- Kučerka, N., Kiselev, A.M., Balga, P. 2004a. Determination of the bilayer thickness and lipid surface area in unilamellar dimyristoylphosphatidylcholine vesicles from small-angle neutron scattering curves: A comparison of evaluation methods. *Eur. Biophys. J.* **33**:328–334
- Kučerka, N., Liu, Y., Chu, N., Petrache, H.I., Tristram-Nagle, S., Nagle, J.F. 2005. Structure of fully hydrated fluid phase DMPC and DLPC lipid bilayers using X-ray scattering from oriented multilamellar arrays and from unilamellar vesicles. *Biophys. J.* **88**:2626–2637
- Kučerka, N., Nagle, J.F., Feller, S.E., Balgavý, P. 2004b. Models to analyze small-angle neutron scattering from unilamellar lipid vesicles. *Phys. Rev. E* **69**:051903 (1–9)
- Kučerka, N., Uhríkova, D., Teixeira, J., Balgavý, P. 2004c. Bilayer thickness in unilamellar phosphatidylcholine vesicles: Small-angle neutron scattering using contrast variation. *Physica B* **350**:e639–e642
- Lewis, B.A., Engelman, D.M. 1983. Lipid bilayer thickness varies linearly with acyl chain length in fluid phosphatidylcholine vesicles. *J. Mol. Biol.* **166**:211–217
- Lewis, R.N.A.H., Sykes, B.D., McElhaney, R. 1988. Thermotropic phase-behavior of model membranes composed of phosphatidylcholines containing *cis*-monounsaturated chain homologs of oleic acid-differential scanning calorimetry and ³¹P NMR spectroscopic studies. *Biochemistry* **27**:880–887
- Liu, Y., Nagle, J.F. 2004. Diffuse scattering provides material parameters and electron density profiles of biomembranes. *Phys. Rev. E* **69**:040901 (1–4)
- Lyatskaya, J., Liu, Y., Tristram-Nagle, S., Katsaras, J., Nagle, J.F. 2001. Method for obtaining structure and structure interactions from oriented lipid bilayers. *Phys. Rev. E* **63**:011907 (1–9)
- Nagle, J.F., Tristram-Nagle, S. 2000. Structure of lipid bilayers. *Biochim. Biophys. Acta* **1469**:159–195
- Nagle, J.F., Wiener, M.C. 1988. Structure of fully hydrated bilayer dispersions. *Biochim. Biophys. Acta* **942**:1–10
- Nagle, J.F., Zhang, R., Tristram-Nagle, S., Sun, W.-J., Petrache, H.I., Suter, R.M. 1996. X-ray structure determination of fully hydrated L-alpha phase dipalmitoylphosphatidylcholine bilayers. *Biophys. J.* **70**:1419–1431
- Needham, D., Evans, E. 1988. Structure and mechanical properties of giant lipid (DMPC) vesicle bilayers from 20°C below to 10°C above the liquid crystal-crystalline phase transition at 24°C. *Biochemistry* **27**:8261–8269
- Pabst, G., Rappolt, M., Amenitsch, A., Laggner, P. 2000. Structural information from multilamellar liposomes at full hydration: Full q-range fitting with high quality X-ray data. *Phys. Rev. E Stat Nonlin Soft Matter Phys* **62**:4000–4009
- Perly, B., Smith, I.P., Jarrell, H.C. 1985. Effects of the replacement of a double bond by a cyclopropane ring in phosphatidylethanolamines: A ²H NMR study of phase transitions and molecular organization. *Biochemistry* **24**:1055–1063
- Petrache, H.I., Feller, S.E., Nagle, J.F. 1997. Determination of component volumes of lipid bilayers from simulations. *Biophys. J.* **72**:2237–2242
- Petrache, H.I., Tristram-Nagle, S., Nagle, J.F. 1998. Fluid phase structure of EPC and DMPC bilayers. *Chem. Phys. Lipids* **95**:83–94
- Rand, R.P., Parsegian, V.A. 1989. Hydration forces between phospholipid bilayers. *Biochim. Biophys. Acta* **988**:351–376
- Rawicz, W., Olbrich, K.C., McIntosh, T., Needham, D., Evans, E. 2000. Effect of chain length and unsaturation on elasticity of lipid bilayers. *Biophys. J.* **79**:328–339
- Seelig, A., Seelig, J. 1977. Effect of a single *cis* double bond on the structure of a phospholipid bilayer. *Biochemistry* **16**:45–49
- Tattre, N.H., Bennett, J.R., Cyr, R. 1968. Maximum and minimum values for lecithin classes from various biological sources. *Biochemistry* **46**:819–829
- Torbet, J., Wilkins, M.H.F. 1976. X-ray diffraction studies of lecithin bilayers. *J. Theor. Biol.* **62**:447–458
- Tristram-Nagle, S., Liu Legleiter, Y. J., Nagle, J.F. 2002. Structure of gel phase DMPC determined by X-ray diffraction. *Biophys. J.* **83**:3324–3335
- Tristram-Nagle, S., Petrache, H.I., Nagle, J.F. 1998. Structure and interactions of fully hydrated dioleoylphosphatidylcholine bilayers. *Biophys. J.* **75**:917–925
- Tristram-Nagle, S., Zhang, R., Suter, R.M., Worthington, C.R., Sun, W.-J., Nagle, J.F. 1993. Measurement of chain tilt angle in fully hydrated bilayers of gel phase lecithins. *Biophys. J.* **64**:1097–1109
- Wiener, M.C., Suter, R.M., Nagle, J.F. 1989. Structure of the fully hydrated gel phase of DPPC. *Biophys. J.* **55**:315
- Wiener, M.C., White, S.H. 1992. Structure of fluid dioleoylphosphatidylcholine bilayer determined by joint refinement of X-ray and neutron diffraction data. II. Distribution and packing of terminal methyl groups. *Biophys. J.* **61**: 428–433
- Zhang, R.S., Tristram-Nagle, S., Sun, W.-J., Headrick, R.L., Irving, T.C., Suter, R.M., Nagle, J.F. 1996. Small-angle X-ray scattering from lipid bilayers is well described by modified Caillé theory but not by paracrystalline theory. *Biophys. J.* **70**: 349–357